Páez Chávez, J.; Wijaya, KP.; Pinto, CM.; Burgos-Simon, C. (2022). A model for type I diabetes in an HIV-infected patient under highlyactive antiretroviral therapy. Chaos, Solitons and Fractals. 155:1-15. https://doi.org/10.1016/j.chaos.2021.111716

A model for type I diabetes in an HIV-infected patient under highly active antiretroviral therapy

Joseph Páez Chávez [a, e], Karunia Putra Wijaya [b], Carla M.A. Pinto [c, *], Clara Burgos-Simón [d]

[a] Center for Applied Dynamical Systems and Computational Methods (CADSCOM), Faculty of Natural Sciences and Mathematics, Escuela Superior Politécnica del Litoral, P.O. Box 09-01-5863, Guayaquil, Ecuador

[b] Mathematical Institute, University of Koblenz-Landau, Universitätstr. 1, D-56070 Koblenz, Germany

[c] School of Engineering, Polytechnic of Porto, and Centre for Mathematics of the University of Porto, Rua Dr. António Bernardino de Almeida 431, 4249-015 Porto, Portugal

[d] Institute for Multidisciplinary Mathematics, Polytechnic University of Valencia, Camino de Vera, 46022 Valencia, Spain

[e] Center for Dynamics, Department of Mathematics, TU Dresden, D-01062 Dresden, Germany

A B S T R A C T

Type 1 diabetes (T1D), previously known as juvenile diabetes or insulin-dependent diabetes, is an autoimmune disease characterized by the insufficient (or lack of) production of insulin by the pancreas. Insulin is crucial to maintain blood sugar at healthy levels. High blood sugar damages the body and causes a variety of symptoms, ranging from severe thirst, fatigue, to urinary infections. The cells responsible for the production of insulin are the β-cells. In T1D, these are killed by an abnormal response of the immune system. Specific clones of cytotoxic T-cells invade the pancreatic islets of Langerhans, and eliminate them. T1D diabetes may develop in human immunodeficiency virus (HIV)-infected patients, though in rare situations. In this paper, we propose a cell model for the development of T1D in these patients, after immune restoration, during highly active antiretroviral therapy (HAART). The study includes the derivation of the qualitative properties of the model, and its comprehensive investigation via path-following methods, using the continuation platform COCO. In this way, the main theoretical predictions are verified in detail. Furthermore, this numerical part establishes accurate parameter thresholds to ensure an effective disease treatment in HIV-infected persons to prevent the development of T1D.

1. Introduction

Diabetes Mellitus (DM) is a chronic metabolic disease diagnosed by high blood glucose levels (known as hyperglycemia). There are three main types of diabetes, namely type 1, type 2, and gestational. In type 1 diabetes (T1D), the immune system identifies the insulin-producing cells (β cells) as external or foreign. This leads to an abnormal immune response, characterized by the inability of the regulatory T cells to control cytotoxic T cells, directed against self-proteins. CD4 and CD8 T cells attack and destroy β cells, and concurrently, the B cells produce antibodies against β cell proteins. There may be some replacement of β cells' numbers by cell division or cell formation; nevertheless, as years go by, the depletion of these cells surmounts the replenishment. A reduction of approximately 80% of β cells is a synonym for the inability of the body to secrete enough insulin, blood sugar levels increase, and clinical diabetes is diagnosed. T1D is responsible for causing severe damage to the body and failure of various organs and tissues. Symptoms include extreme thirst and hunger, dry mouth, upset stomach and vomiting, urge to urinate, weight loss, fatigue, blurry vision, Kussmal respiration, infections of your skin, urinary tract, or vagina, mood changes, amongst others. Access to treatment and insulin for T1D patients is life-saving [1].

The most common type of diabetes is type 2. It occurs mainly in adults and results from the body becoming resistant or not producing enough insulin. The third type of diabetes is gestational. It develops during pregnancy and may cause medical complications to the mother and fetus. It is likely to disappear after pregnancy, but the affected women and their children have a higher risk of developing type 2 diabetes in the future. Treatment for diabetes is a healthy lifestyle, which includes exercise, a healthy diet, maintain a normal body weight, avoid tobacco, regular

screening, and medication and/or insulin to restore blood glucose levels [2].

The number of people with diabetes is dramatically increasing since 1980 from 108 million to 422 million in 2014. The prevalence of diabetes in adults has almost doubled in this period, from 4.7% to 8.5%. This increase is more severe in the middle- and low-income countries due to bad economics and health systems [3]. The death rate attributed to diabetes is high, with an estimated 1.6 million diabetic deaths in 2016. This corresponds to nearly the total number of deaths due to high blood glucose in people below 70 years old. In 2016, the World Health Organization (WHO) considered diabetes the seventh leading cause of death. The recent number from 2019 unraveled approximately 463 million adults living with diabetes, and this number is predicted to tragically rise to 700 million by 2045. People living with T1D are approximately 5%-10% of the total number of diabetics. In the United States of America, 1.6 million people have T1D, and is estimated a 5 million new diagnosis of T1D by 2050. Two hundred thousand American children and teenagers have T1D. In the United Kingdom, 3.7 million people have diabetes, of which 10% are of type 1. Twenty nice thousand children have T1D [4]. T1D prevalence and incidence are also increasing worldwide, which will cause an even major burden to low and middle-income countries [5]. There is, though, a globally agreed target to halt the rise in diabetes and obesity by 2025, which may help prevent these horrible numbers [3,6].

The human immunodeficiency virus (HIV) is a lentivirus, belonging to the family of *Retroviridae*. Typical viruses are characterized by a long incubation period (months, or years) and induce a broader range of pathologies in several animal species. Lentiviruses are one of the most used vectors for gene transfer due to their flexible genome and transducing properties. HIV attacks preferentially the $CD4^+$ T cells, major components of our immune system. This unbalances the immune system, undermining an effective response to pathogens. Over time, opportunistic infections and/or cancers develop, defining the last stage of the infection by HIV, which is called Acquired Immune deficiency Syndrome (AIDS). There is no cure for HIV infection currently; nevertheless, HIV infection is considered a chronic disease. The substantial development of medicines, called antiretroviral therapies (ARTs), has given hope to HIV patients, who can now live longer and healthier lives [7].

In 2020, an estimated 37.7 million people were living with HIV worldwide [8], of which 25.4 million are in the WHO African Region. Only 27.5 million had access to ART. More than 36 million died from AIDS till now. In 2020, more than 1.5 million people were diagnosed with HIV infection. AIDS-related diseases contributed to 680 000 deaths. HIV prevention methods and interventions vary according to the patient and include male and female condoms, the use of ART and pre-exposure prophylaxis (PrEP), voluntary male medical circumcision (VMMC), behavior change interventions to reduce the number of sexual partners, the use of clean needles and syringes, opiate substitution therapy, and the treatment of HIV-infected people, to reduce viral load and, thus, onward transmission. Although the efficacy and diversity of prevention measures, the new infections among adults is not decreasing globally. Three main reasons are behind this, starting from the absence of a strong political commitment, inadequate information campaigns about sexual behavior, reproductive needs and rights, and weak systematic implementation of prevention measures [9].

Diabetes (type 2) has a higher prevalence among pre-ART HIV-infected patients. Moreover, more educated, hypertensive, and obese HIV-infected adults are also more prone to have type 2 diabetes, as co-morbidity [10]. In this scope, in the last few decades, the application of statistical mathematical models has increased to understand the dynamics of type 2 diabetes and HIV infection better [11–13]. Nevertheless, the literature on models discussing the behavior of HIV-infection dynamics and T1D is scarce. In 2007, Mahaffy *et al.* [14] propose a model for the dynamics of the immune response in autoimmune diabetes (T1D). The authors explain T-cell activation as an increasing function of the autoantigen level, whereas decreasing levels lead to the production of memory cells. Moreover, high β-cells death rates increase autoantigen levels, which turn off memory cells production, leading to less activated T cells. After clearance of the peptide, the production of memory cells is recovered, and the cycle repeats. Magombedze *et al.* [15] formulate a mathematical model that incorporates the role of cytotoxic T cells and regulatory T cells in T1D diabetes. Numerical results indicate that high levels of regulatory T cells reduce the activity of auto-reactive T cells, permitting β-cells to replenish and allow insulin production. In 2012, Marinkovic *et al.* [16] suggest a model for the dynamics of DM, which includes metabolism and the immune system at early stages of the disease. The model fits well clinical and non-clinical data and suggests that amplitude and duration of autoimmune response may explain β-cell loss. The authors in [17] perform the bifurcation analysis for a known mathematical model for the early stages of T1D. Several innovative treatment strategies are proposed, such as increasing the phagocytic ability of resting or activated macrophages. Carvalho *et al* [18] describe a non-integer order model for T1D, focusing on the role of macrophages from non-obese diabetic (NOD) mice and from control (Balb/c) mice in triggering autoimmune T1D. The results obtained showed persistence of inflammation for NOD and control mice, for smaller values of the order of the fractional derivative. This adds richness to the behavior of the model since this is not observed for the integer-order model. In the literature, T1D diabetes was reported to develop in HIV-infected patients after immune restoration during antiretroviral therapy [19,20]. In 1998 [19], the authors report an 18-year-old HIV-infected teenager who developed new-onset insulin-dependent diabetes mellitus in association with anemia. The authors pinpoint the progression of hyperglycemia associated with a rapid increase in insulin requirement, as indicative of insulin resistance. In [20], antibodies to glutamic acid decarboxylase, were detected in three HIV patients in Japan, with no prior T1D disease, at a time when CD4 cell counts rose abruptly. It is believed that immune restoration turns patients vulnerable to T1D. In 2015, another case study was reported in [21]. This described the clinical outcome of a previously healthy 40-year-old man infected with HIV and then developed newly-onset T1D after immune restoration following antiretrovial therapy. The authors refer to ethnicity as a preponderant factor for this diagnosis, highlighting Japanese people as more susceptible than white patients. Shimoyama *et al.* [22] describe the sudden development of fulminant T1D (FT1D) in a patient diagnosed with AIDS. FT1D is defined by the abrupt onset of insulin-deficient severe hyperglycemia, diabetic ketoacidosis (DKA), high serum pancreatic enzyme levels, and no diabetes-related autoantibodies. The authors discuss HIV/AIDS and FT1D association, the FT1D onset despite negative CMV antigenemia, and the cause of severe hypoglycemia during the course of FT1D. Recently, in 2020 [23], the authors report the case of an older African American man who developed T1D in a state of immune reconstitution after antiretroviral therapy.

With the aforementioned ideas in mind, in this paper, we propose a within-host mathematical model for the dynamics of T1D in HIV-infected patients. In Section 2, we describe the ordinary differential equations composing the model. This is followed in Section 3, by the study of the qualitative properties of the model. In Section 4, we investigate the dynamical behavior of the equilibria under variation of relevant disease control parameters. We end this work with the main conclusions of this study and future research lines.

2. Description of the model

The model is composed by the concentration of healthy CD4$^+$ T cells T, infected CD4$^+$ T cells I, HIV viruses V, resting macrophages M, activated macrophages M_a, infected macrophages M_i, apoptotic β-cells B_a, necrotic β-cells B_n and cytokines C. The model is an adaptation of a basic HIV model and a macrophage-induced inflammation model [24,25]. The basic HIV model consists of three compartments, one for the CD4$^+$ T cells population, one for the infected CD4$^+$ T cells population, and another one for the HIV viral load [24]. During HIV infection, macrophages can also be infected by HIV [26], thus we have added equations modeling this behaviour in our derived model. The macrophages-induced inflammation model, proposed in [25], tries to provide a biological explanation to the triggering of autoimmune T1D in non-obese diabetic mice (NOD). Its derivation considers the slower activation rate of macrophages in NOD, when compared to control (Balb/c) mice, as the major responsible for the onset of T1D. Thus, the authors quantify variables from the Copenhagen model [27], based on parameters coming from experimental data for the two groups of mice, revise it to obtain a reasonable model. They conclude the apoptotic wave may induce inflammatory response in NOD but not in Balb/c mice, since macrophages are extremely fast in clearing that wave in the later. Clinically, the literature is scarce in evidence of the development of T1D in HIV infected patients. There is solely a handful of cases concerning the onset of T1D in HIV infected patients after immune restoration. To the best of our knowledge, there are no published references on mathematical models of this epidemiological phenomenon. In the derivation of our model, we consider the well-known model of the within-host dynamics of HIV, considering CD4$^+$ T cells, and we add to it macrophages. To this sub-model, we agglutinate the dynamics of the model developed in [25] for the onset of T1D diabetes in mice. We consider the neonatal wave, $W(t)$, for two main reasons. This wave is observed in neonatal babies [28], and, second, it is known that an adult will have in his body both newborn and older beta cells [29]. Thus, we are assuming an analogous phenomenon as the one seen in mice, with the addition of the T cells. I.e., a unique conjunction of the increase in CD4$^+$ T cells counts, resulting from immune restoration, and the macrophages immune roles would trigger a "neonatal" wave, inducing inflammation and self antigen presentation, and prompting T1D in HIV infected patients after immune restoration. We proceed with the details of the derived equations below.

Healthy T cells T are created at thymus with a rate s (Eq. (2.2)). They can also generate from the proliferation of existing T cells. This is represented by a logistic function in which p is the maximum proliferation rate and $T_{\max}$ is the T cells maximum density. T cells are removed at rate δ_1. T cells are infected by HIV at a rate kVT and move to the class of infected T cells I (Eq. 2.3). Reverse transcriptase inhibitor efficacy is included in the CD4$^+$ T cells equations by the parameter $0 \leq \epsilon_{RT} \leq 1$. One means 100% treatment efficacy. HIV-infected T cells I are removed at rate δ_2. The viruses V are produced by the infected CD4$^+$ T cells I and infected macrophages M_i with bursting sizes N_1 and N_2, respectively (Eq. (2.4)). The factor $(1-\epsilon_P)$ reduces viral load due to the protease inhibitor efficacy $0 \leq \epsilon_P \leq 1$. The viruses are removed at a rate c. The resting macrophages M enter the tissue at a constant rate J, and leave randomly with mean residence time $1/\delta_3$ (Eq. (2.5)). They are activated through contact with apoptotic cells B_a at a rate g. Activated macrophages M_a recruit macrophages to the tissue at a rate b (Eq. (2.6)). They can be infected by HIV at a rate m and move to the infected class M_i as well as die at a rate δ_4. The infected macrophages M_i are removed at rate δ_5 (Eq. (2.7)). Parameters e_i for $i = 1,\ 2,\ 3$ model the crowding effects, described by reduced entry and/or increased efflux of macrophages from tissue at high densities. The β-cells' cytokine-induced apoptosis elimination rate is represented by a Michäelis-Menten saturated function of C, with a maximal rate $A_{\max}$, and a half-max cytokine concentration k_c (Eq. 2.8). Apoptotic β-cells B_a follow a neonatal wave

$$W(t) = 4 \times 10^7 \exp\left[-\left(\frac{t-9}{3}\right)^2\right] \tag{2.1}$$

and are removed by resting, activated, and infected T cells and macrophages, at rates f_1, f_2, and f_3, respectively. They become necrotic β- cells B_n at a rate δ_6 (Eq. (2.9)). The cytokines C are produced by the necrotic cells B_n and the healthy and infected T cells as well as activated and infected macrophages at a rate α, and are removed at a rate δ_7 (Eq. (2.10)). The nonlinear system of differential equations describing the dynamics of the model is given by

$$\frac{dT}{dt} = s + pT\left(1 - \frac{T}{T_{max}}\right) - \delta_1 T - k(1-\epsilon_{RT})VT, \tag{2.2}$$

$$\frac{dI}{dt} = k(1-\epsilon_{RT})VT - \delta_2 I, \tag{2.3}$$

$$\frac{dV}{dt} = N_1\delta_2(1-\epsilon_P)I + N_2\delta_5(1-\epsilon_P)M_i - cV, \tag{2.4}$$

$$\frac{dM}{dt} = J + (\delta_4 + b)M_a - \delta_3 M - gMB_a - e_1 M(M + M_a + M_i), \tag{2.5}$$

$$\frac{dM_a}{dt} = gMB_a - \delta_4 M_a - e_2 M_a(M + M_a + M_i) - kM_aV, \tag{2.6}$$

$$\frac{dM_i}{dt} = kM_aV - e_3 M_i(M + M_a + M_i) - \delta_5 M_i, \tag{2.7}$$

$$\begin{aligned}\frac{dB_a}{dt} &= W(t) + \frac{A_{max}C}{k_c + C} - f_1(T+M)B_a \\ &\quad - f_2 M_a B_a - f_3(I + M_i)B_a - \delta_6 B_a,\end{aligned} \tag{2.8}$$

$$\frac{dB_n}{dt} = \delta_6 B_a - f_1(T+M)B_n - f_2 M_a B_n - f_3(I+M_i)B_n, \tag{2.9}$$

$$\frac{dC}{dt} = \alpha B_n(T + I + M_a + M_i) - \delta_7 C. \tag{2.10}$$

The schematic diagram of model (2.2)–(2.10) can be found in Fig. 2.1.

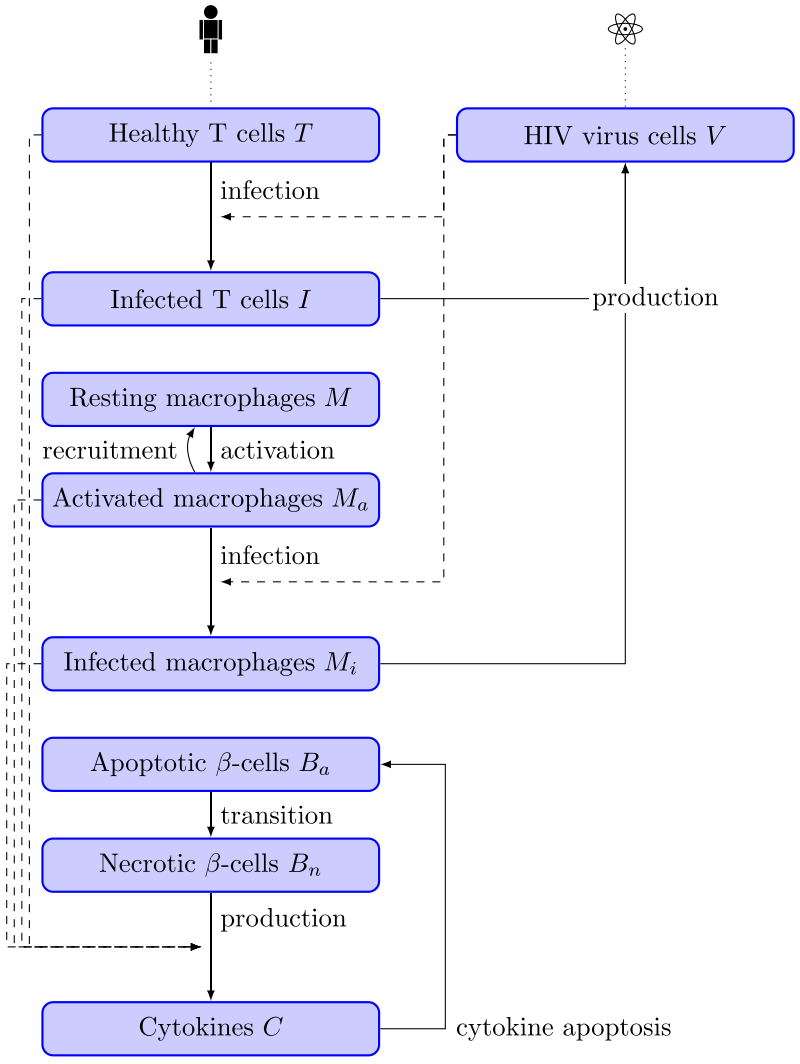

Fig. 2.1. Schematic transmission diagram describing the model (2.2)–(2.10).

3. Qualitative properties of the model

A short observation to the model (2.2)–(2.10) suggests that every unit normal of the boundary of the nonnegative nonant $\mathbb{R}^9_+$ possesses a right-to-obtuse angle against the vector field at the corresponding boundary. This leads to nonnegative trajectories of the model system for all time providing that the initial condition is also nonnegative. Along with the invariance, this section is devoted to analyzing the behavior of the model system after long time whereby the neonatal wave for apoptotic β-cells turns to be negligible, i.e., $W \simeq 0$. In this case, the asymptotic behavior of the model (2.2)–(2.10) becomes independent of W. In the sequel, we will see at least numerically that the model system (2.2)–(2.10) admits four equilibria, namely disease-free, T1D-free, HIV-free, and T1D and HIV coexistence equilibria. Due to complexity, in what follows we can only afford explicit formulations of the disease-free and T1D-free equilibrium.

3.1. Disease-free equilibrium

Our main goal here is to see mathematically, to what extent reverse transcriptase inhibitor and protease inhibitor may be able to drive the system solutions toward the disease-free equilibrium

$$\mathscr{E}_{\text{DFE}} = (T_0, 0, 0, M_0, 0, 0, 0, 0, 0).$$

According to (2.2), the equilibrium state T_0 satisfies $-\frac{p}{T_{\max}}T^2 + (p - \delta_1)T + s = 0$. This is a parabolic function with two real-valued roots of opposed signs. Clearly is one positive equilibrium state present. Similarly, one real positive root M_0 of $-e_1M^2 - \delta_3 M + J = 0$ also exists. The Jacobian matrix of the vector field evaluated at the disease-free equilibrium takes the form

$$\mathcal{J}(\mathscr{E}_{\text{DFE}}) = \begin{pmatrix} \mathcal{J}_{11} & 0 & \mathcal{J}_{13} & 0 & 0 & 0 & 0 & 0 & 0 \\ 0 & -\delta_2 & -\mathcal{J}_{13} & 0 & 0 & 0 & 0 & 0 & 0 \\ 0 & \mathcal{J}_{32} & -c & 0 & 0 & \mathcal{J}_{36} & 0 & 0 & 0 \\ 0 & 0 & -m_1M_0 & -\delta_3 - 2e_1M_0 & \mathcal{J}_{45} & -e_1M_0 & -gM_0 & 0 & 0 \\ 0 & 0 & 0 & 0 & -\delta_4 - e_2M_0 & 0 & gM_0 & 0 & 0 \\ 0 & 0 & 0 & 0 & 0 & -\delta_5 - e_3M_0 & 0 & 0 & 0 \\ 0 & 0 & 0 & 0 & 0 & 0 & \mathcal{J}_{77} & 0 & \frac{A_{max}}{k_c} \\ 0 & 0 & 0 & 0 & 0 & 0 & \delta_6 & -f_1(T_0 + M_0) & 0 \\ 0 & 0 & 0 & 0 & 0 & 0 & 0 & \alpha T_0 & -\delta_7 \end{pmatrix}$$

where

$$\mathcal{J}_{11} = -2\frac{pT_0}{T_{max}} + (p - \delta_1), \quad \mathcal{J}_{13} = -k(1-\epsilon_{RT})T_0, \quad \mathcal{J}_{32} = N_1\delta_2(1-\epsilon_P),$$
$$\mathcal{J}_{36} = N_2\delta_5(1-\epsilon_P), \qquad \mathcal{J}_{45} = \delta_4 + b - e_1M_0, \quad \mathcal{J}_{77} = -\delta_6 - f_1(T_0+M_0).$$

Since $\mathcal{J}_{11}$ returns from the derivative of a concave quadratic function evaluated at its positive root, it obviously holds $\mathcal{J}_{11} < 0$. Using the cofactor method for the determinant of $\mathcal{J}(\mathscr{E}_{\mathrm{DFE}}) - \lambda\,\mathrm{id}$, it is verifiable that the following are the eigenvalues of the Jacobian matrix in the order of reading: $\mathcal{J}_{11}$, $-\delta_3 - 2e_1M_0$, $-\delta_4 - e_2M_0$, and $-\delta_5 - e_3M_0$. The remaining eigenvalues are those of

$$\begin{pmatrix} -\delta_2 & -\mathcal{J}_{13} \\ \mathcal{J}_{32} & -c \end{pmatrix} \quad \text{and} \quad \begin{pmatrix} \mathcal{J}_{77} & 0 & \frac{A_{max}}{k_c} \\ \delta_6 & -f_1(T_0+M_0) & 0 \\ 0 & \alpha T_0 & -\delta_7 \end{pmatrix},$$

respectively. The first matrix gives the negative summation of the eigenvalues by the trace, and all the eigenvalues have negative real parts providing that the determinant is positive. The second matrix gives positive coefficients of the characteristic polynomial, providing that the determinant is also positive. Accordingly, the trinomial takes a positive value at zero, is increasing and convex on the positive abscissa, and therefore can only have roots of negative real parts. The preceding statements about the determinants can be translated as follows: stable submanifolds around $\mathscr{E}_{\mathrm{DFE}}$ in the (I,V)- and (B_a,B_n,C)-space are formed in case

$$\mathcal{R}^2_{\mathrm{HD}} := \frac{k(1-\epsilon_{RT})T_0}{c}\cdot\frac{N_1\delta_2(1-\epsilon_P)}{\delta_2}$$
$$= \frac{k(1-\epsilon_{RT})\left[\frac{(p-\delta_1)+\sqrt{(p-\delta_1)^2+4ps/T_{max}}}{2p/T_{max}}\right]}{c}\cdot\frac{N_1\delta_2(1-\epsilon_P)}{\delta_2} < 1 \tag{3.1}$$

and

$$\mathcal{R}^3_{\mathrm{TD}} := \frac{\alpha T_0}{f_1(T_0+M_0)}\cdot\frac{A_{max}}{k_c\delta_7}\cdot\frac{\delta_6}{f_1(T_0+M_0)+\delta_6}$$
$$= \frac{\alpha\left[\frac{(p-\delta_1)+\sqrt{(p-\delta_1)^2+4ps/T_{max}}}{2p/T_{max}}\right]}{f_1\left[\frac{(p-\delta_1)+\sqrt{(p-\delta_1)^2+4ps/T_{max}}}{2p/T_{max}}+\frac{-\delta_3+\sqrt{\delta_3^2+4e_1J}}{2e_1}\right]}\cdot\frac{A_{max}}{k_c\delta_7}$$
$$\cdot\frac{\delta_6}{f_1\left[\frac{(p-\delta_1)+\sqrt{(p-\delta_1)^2+4ps/T_{max}}}{2p/T_{max}}+\frac{-\delta_3+\sqrt{\delta_3^2+4e_1J}}{2e_1}\right]+\delta_6} < 1, \tag{3.2}$$

respectively. When one inequality changes in direction, $\mathscr{E}_{\mathrm{DFE}}$ is in the configuration of a saddle node, making one disease a source of endemicity.

One can biologically understand all the above expressions in the following way. For example, the expression $k(1-\epsilon_{RT})T_0$ appears as an inflow in the compartment I where $V=1$ and $T=T_0$, and $1/c$ as the virus lifespan. Therefore, the first expression in $\mathcal{R}^2_{\mathrm{HD}}$, $k(1-\epsilon_{RT})T_0/c$, represents the number of newly infected T cells generated by one virus cell per average virus lifespan, when all T cells are still healthy. Similarly, the second expression $N_1\delta_2(1-\epsilon_P)/\delta_2$ represents the number of new virus cells generated by one apoptotic T cell per average infected cell's lifespan. The square and cubic root take the geometric average of different proportions that were equipped by different time scales. All these basic reproductive numbers have been defined in the same way as in [35], which characterize certain thresholds at which the disease-free equilibrium is at the interface of different stability statuses.

To our aim for this section, observe that even $\epsilon_{RT} = \epsilon_P = 1$ from both inhibitors does not guarantee the local stability of $\mathscr{E}_{\mathrm{DFE}}$ unless the basic reproductive number related to T1D, $\mathcal{R}_{\mathrm{TD}}$, is also suppressed below one.

3.2. T1D-Free equilibrium

This equilibrium, henceforth denoted by

$$\mathscr{E}_{\text{T1D}} = (T_1, I_1, V_1, M_1, 0, 0, 0, 0, 0),$$

refers to a state where an HIV patient with co-morbidity is eventually released from T1D infection but remains HIV-viremic. As also highlighted previously, we would like to see if reverse transcriptase inhibitor and protease inhibitor may play a considerable role in steering the model dynamics toward this equilibrium. From the constancy of I_1 and V_1, it holds according to (2.3) and (2.4) that

$$\frac{I_1}{V_1} = \frac{c}{N_1\delta_2(1-\epsilon_P)} = \frac{k(1-\epsilon_{RT})T_1}{\delta_2}, \tag{3.3}$$

which gives us T_1. From (2.2) and T_1, we get

$$V_1 = \frac{\frac{s}{T_1} + p\left(1-\frac{T_1}{T_{max}}\right) - \delta_1}{k(1-\epsilon_{RT})}. \tag{3.4}$$

Note that $\mathscr{E}_{\text{T1D}}$ is not always biologically relevant as the state V_1 can be negative when ϵ_{RT} and ϵ_P are relatively large. Finally, Eq. (2.5) returns a positive M_1 that solves the equation $-e_1M^2 - \delta_3 M + J = 0$. Under similar notations as before, the Jacobian matrix of the vector field evaluated at the T1D-free equilibrium reads as

$$\mathcal{J}(\mathscr{E}_{\text{T1D}}) = \begin{pmatrix} \mathcal{J}_{11} & 0 & \mathcal{J}_{13} & 0 & 0 & 0 & 0 & 0 & 0 \\ -\mathcal{J}_{13}\frac{V_1}{T_1} & -\delta_2 & -\mathcal{J}_{13} & 0 & 0 & 0 & 0 & 0 & 0 \\ 0 & \mathcal{J}_{32} & -c & 0 & 0 & \mathcal{J}_{36} & 0 & 0 & 0 \\ 0 & 0 & -m_1M_1 & \mathcal{J}_{44} & \mathcal{J}_{45} & -e_1M_1 & -gM_1 & 0 & 0 \\ 0 & 0 & 0 & 0 & \mathcal{J}_{55} & 0 & gM_1 & 0 & 0 \\ 0 & 0 & 0 & 0 & kV_1 & -\delta_5 - e_3M_1 & 0 & 0 & 0 \\ 0 & 0 & 0 & 0 & 0 & 0 & \mathcal{J}_{77} & 0 & \frac{A_{max}}{k_c} \\ 0 & 0 & 0 & 0 & 0 & 0 & \delta_6 & \mathcal{J}_{88} & 0 \\ 0 & 0 & 0 & 0 & 0 & 0 & 0 & \alpha(T_1+I_1) & -\delta_7 \end{pmatrix} \tag{3.5}$$

where

$$\mathcal{J}_{11} = -2\frac{pT_1}{T_{max}} + (p-\delta_1) - k(1-\epsilon_{RT})V_1, \quad \mathcal{J}_{13} = -k(1-\epsilon_{RT})T_1, \quad \mathcal{J}_{32} = N_1\delta_2(1-\epsilon_P),$$
$$\mathcal{J}_{36} = N_2\delta_5(1-\epsilon_P), \quad \mathcal{J}_{44} = -\delta_3 - 2e_1M_1 - m_1V_1, \quad \mathcal{J}_{45} = \delta_4 + b - e_1M_1,$$
$$\mathcal{J}_{55} = -\delta_4 - e_2M_1 - kV_1, \quad \mathcal{J}_{77} = -\delta_6 - f_1(T_1+M_1) - f_3I_1, \quad \mathcal{J}_{88} = \mathcal{J}_{77} + \delta_6.$$

Eqs. (3.3) and (3.4) evoke $c\delta_2 = -\mathcal{J}_{13}\mathcal{J}_{32}$ and $\mathcal{J}_{11} = -s/T_1 - pT_1/T_{\max} < 0$.

For the sake of abbreviation, the preceding Jacobian matrix is rewritten in terms of block matrices as follows

$$\mathcal{J}(\mathscr{E}_{\text{T1D}}) = \begin{pmatrix} B_1 & 0 & B_2 \\ B_3 & \mathcal{J}_{44} & B_4 \\ 0 & 0 & B_5 \end{pmatrix}. \tag{3.6}$$

Note that the first block matrix B_1 spans the first three rows and columns of the Jacobian matrix. Since

$$\begin{pmatrix} B_3 \\ 0 \end{pmatrix} B_1^{-1} = 0,$$

it thus holds

$$\det \mathcal{J}(\mathscr{E}_{\text{T1D}}) = \det B_1 \cdot \det\left\{ \begin{pmatrix} \mathcal{J}_{44} & B_4 \\ 0 & B_5 \end{pmatrix} - \begin{pmatrix} B_3 \\ 0 \end{pmatrix} B_1^{-1} \begin{pmatrix} 0 & B_2 \end{pmatrix} \right\} = \det B_1 \cdot \mathcal{J}_{44} \cdot \det B_5.$$

The eigenvalues of the Jacobian matrix are then $\mathcal{J}_{44}$ and those of B_1 and B_5. The block matrix B_1 has positive coefficients of the characteristic polynomial without further confirmation except the constant term, which is given by $\mathcal{J}_{13}^2\mathcal{J}_{32}V_1/T_1 - \mathcal{J}_{11}c\delta_2 - \mathcal{J}_{11}\mathcal{J}_{13}\mathcal{J}_{32} = \mathcal{J}_{13}^2\mathcal{J}_{32}V_1/T_1$. This is indeed a positive number. Therefore, the model system acquires a stable submanifold around the T1D-free equilibrium in the (T, I, V)-space. Moreover, the block matrix B_5 corresponds to the contribution of T1D. The eigenvalues are $\mathcal{J}_{55}$, $-\delta_5 - e_3M_1$, and those of

$$\begin{pmatrix} \mathcal{J}_{77} & 0 & \frac{A_{max}}{k_c} \\ \delta_6 & \mathcal{J}_{88} & 0 \\ 0 & \alpha(T_1+I_1) & -\delta_7 \end{pmatrix}.$$

This matrix possesses positive coefficients of the characteristic polynomial, providing that its determinant is positive or

$$\begin{aligned} \mathcal{R}_{\text{TT}}^3 &:= \frac{\alpha(T_1+I_1)}{-\mathcal{J}_{88}} \cdot \frac{A_{max}}{k_c\delta_7} \cdot \frac{\delta_6}{-\mathcal{J}_{77}} \\ &= \frac{\alpha(T_1+I_1)}{f_1(T_1+M_1)+f_3I_1} \cdot \frac{A_{max}}{k_c\delta_7} \cdot \frac{\delta_6}{f_1(T_1+M_1)+f_3I_1+\delta_6} \\ &= \frac{\alpha\left[\frac{c\delta_2}{k(1-\epsilon_{RT})N_1\delta_2(1-\epsilon_P)} + I_1\right]}{f_1\left[\frac{c\delta_2}{k(1-\epsilon_{RT})N_1\delta_2(1-\epsilon_P)} + \frac{-\delta_3+\sqrt{\delta_3^2+4e_1J}}{2e_1}\right] + f_3I_1} \\ &\quad \cdot \frac{A_{max}}{k_c\delta_7} \cdot \frac{\delta_6}{f_1\left[\frac{c\delta_2}{k(1-\epsilon_{RT})N_1\delta_2(1-\epsilon_P)} + \frac{-\delta_3+\sqrt{\delta_3^2+4e_1J}}{2e_1}\right] + f_3I_1 + \delta_6} < 1 \end{aligned} \tag{3.7}$$

where

$$V_1 = \left[\frac{\frac{sk(1-\epsilon_{RT})N_1\delta_2(1-\epsilon_P)}{c\delta_2} + p\left(1 - \frac{c\delta_2}{T_{max}k(1-\epsilon_{RT})N_1\delta_2(1-\epsilon_P)}\right) - \delta_1}{k(1-\epsilon_{RT})} \right] \text{ and } I_1 = \frac{c}{N_1\delta_2(1-\epsilon_P)}V_1.$$

As we will see later by some numerical investigation, $\mathcal{R}_{\text{TT}}$ increases (decreases) by increasing (decreasing) ϵ_{RT} and ϵ_P when $\mathcal{R}_{\text{TT}} \leq 1$ and when $\mathcal{R}_{\text{TT}}$ shortly exceeds 1. This finding draws out an important biological interpretation. By increasing the efficacies of reverse transcriptase inhibitor and protease inhibitor under improved treatment intensities, we aim to suppress the HIV virus population to a considerably harmless level. However, this also hampers setting to a state where the patient is free from T1D. In the next section, we

will see that this action indeed increases the risk of coexistence of T1D and HIV infection. Of further particular interest in the numerical study is to determine the 'thickness' of such an intermediate window of coexistence before improving both inhibitors brings the patient successfully toward an HIV-free equilibrium. Incorrect treatments may drive a certain state to fall within this window and thus raise careful practical considerations.

3.3. T1D–HIV Coexistence equilibrium

We argue that computing a coexistence equilibrium under direct substitutions from vanishing the vector field of the system (2.2)–(2.10) returns complications. Our alternative way departs from analyzing if a continuum of positive solutions arises from the T1D-free equilibrium $\mathscr{E}_{\cancel{\text{T1D}}}$ and determining which conditions lead to such a branching phenomenon. The previous section hints that $\mathcal{R}_{\text{TT}} \neq 1$ makes the Jacobian matrix non-singular. Moreover, the matrix becomes singular if $\mathcal{R}_{\text{TT}} = 1$. Crandall and Rabinowitz in [36, Theorem 1.2] guarantee that $(\mathscr{E}_{\cancel{\text{T1D}}}, \mathcal{R}_{\text{TT}} \neq 1)$ can never be a branching point, except $(\mathscr{E}_{\cancel{\text{T1D}}}, \mathcal{R}_{\text{TT}} = 1)$. Our next task is to make sure that the latter is indeed a branching point and that the branching solutions go toward the positive nonant in a neighborhood of $\mathscr{E}_{\cancel{\text{T1D}}}$.

In a sufficiently close neighborhood of $\mathscr{E}_{\cancel{\text{T1D}}}$, (2.3) and (2.4) give us

$$\begin{aligned}
T &= \frac{\delta_2 I}{k(1-\epsilon_{RT})V} \\
&= \frac{\delta_2}{k(1-\epsilon_{RT})} \cdot \left[\frac{c}{N_1\delta_2(1-\epsilon_P)} - \frac{N_2\delta_5(1-\epsilon_P)}{N_1\delta_2(1-\epsilon_P)V} M_i \right] \\
&= T_1 - \frac{\delta_2 N_2 \delta_5}{k(1-\epsilon_{RT})N_1\delta_2} \left[\frac{1}{V_1} - \frac{V-V_1}{V_1^2} + \mathcal{O}(|V-V_1|^2) \right] M_i \\
&= T_1 - \frac{\delta_2 N_2 \delta_5}{k(1-\epsilon_{RT})N_1\delta_2 V_1} M_i + \mathcal{O}\left(\left\| \begin{pmatrix} M_i \\ V-V_1 \end{pmatrix} \right\|^2 \right).
\end{aligned}$$

It means that the equilibrium state T decreases from T_1 as M_i rises from 0 to a small positive value. Eq. (2.2) also returns

$$V = \frac{\frac{s}{T} + p\left(1 - \frac{T}{T_{max}}\right) - \delta_1}{k(1-\epsilon_{RT})} = V_1 + \frac{\delta_2 N_2 \delta_5}{k(1-\epsilon_{RT})N_1\delta_2 V_1} \left[\frac{\frac{s}{T_1^2} + \frac{p}{T_{max}}}{k(1-\epsilon_{RT})} \right] M_i + \mathcal{O}\left(\left\| \begin{pmatrix} M_i \\ V-V_1 \end{pmatrix} \right\|^2 \right),$$

which indicates that the virus cells increase in density under the continuous persistence of infected macrophages. The preceding two equations evoke $V - V_1 = \mathcal{O}(|M_i|)$, making the higher order terms $\mathcal{O}\left(|M_i|^2\right)$. In return, the infected T cells also undergo changes in density according to

$$I = \frac{k(1-\epsilon_{RT})}{\delta_2} TV = I_1 + \frac{N_2\delta_5}{N_1\delta_2 V_1} \left[\frac{\frac{s}{T_1} + \frac{pT_1}{T_{max}}}{k(1-\epsilon_{RT})} - V_1 \right] M_i + \mathcal{O}\left(|M_i|^2\right).$$

Observe that the fate of the infected T cells counts on the tradeoff between recruitment rate and proliferation of the healthy T cells as well as the presence of virus. Now the equilibrium state M should satisfy according to (2.5)

$$-e_1 M^2 - (\delta_3 + gB_a + e_1 M_a + e_1 M_i)M + J + (\delta_4 + b)M_a = 0$$

whose positive root is given by

$$\begin{aligned}
M &= \frac{(\delta_3 + gB_a + e_1 M_a + e_1 M_i) - \sqrt{(\delta_3 + gB_a + e_1 M_a + e_1 M_i)^2 + 4e_1[J + (\delta_4 + b)M_a]}}{-2e_1} \\
&= M_1 + \frac{2b + \delta_3 + 2\delta_4 - \sqrt{4Je_1 + \delta_3^2}}{2\sqrt{4Je_1 + \delta_3^2}} M_a + \frac{\delta_3 - \sqrt{4Je_1 + \delta_3^2}}{2\sqrt{4Je_1 + \delta_3^2}} M_i + \frac{g\left(\delta_3 - \sqrt{4Je_1 + \delta_3^2}\right)}{2e_1\sqrt{4Je_1 + \delta_3^2}} B_a \\
&+ \mathcal{O}\left(\left\| \begin{pmatrix} M_a \\ M_i \\ B_a \end{pmatrix} \right\|^2 \right).
\end{aligned}$$

Looking at the numerical values from Table 1, M shall decrease on the rise of M_i and B_a, but increase on the rise of M_a.

For the sake of abbreviation, let us denote $\mathcal{I} := (M_a, M_i, B_a, B_i, C)$. Substituting the previous results to (2.6)–(2.10), we obtain

$$\underbrace{B_5}_{\mathcal{F}-\mathcal{V}} \mathcal{I} + F_2(\mathcal{I}) + \mathcal{O}\left(\|\mathcal{I}\|^3\right) = 0$$

where B_5 is given as in (3.6) and $\mathcal{V}$ denotes the diagonal matrix taking the negative diagonal entries of B_5. In line with [35], $\mathcal{F}$ corresponds to new infection terms in the five states while $\mathcal{V}$ to net transitions. Due to complexity, we shall digress the explicit formulation of the quadratic term F_2 for the moment. Denoting

$$\tilde{\mathcal{I}} := \mathcal{V}\mathcal{I} \tag{3.8}$$

and multiplying the preceding equation with -1, we obtain

$$\varphi(\tilde{\mathcal{I}}) := \tilde{\mathcal{I}} - \mathcal{F}\mathcal{V}^{-1}\tilde{\mathcal{I}} - F_2(\tilde{\mathcal{I}}) + \mathcal{O}\left(\|\tilde{\mathcal{I}}\|^3\right) = 0 \tag{3.9}$$

The format of Eq. (3.9) fits into the canonical form of bifurcation equation in [37,38]. To guarantee the existence of a coexistence equilibrium, the point $(\mathcal{R}_{\mathrm{TT}} = 1, \tilde{\mathcal{I}} = 0)$ is first checked for being a branch point of (3.9). Since $\varphi : \Omega \to \mathbb{R}^5$ is a polynomial on an open neighborhood Ω of $\tilde{\mathcal{I}} = 0$, it holds that $\varphi \in C^\infty(\Omega)$. Let $q \in \mathbb{R}^5$ be a point in the codomain of φ such that $q \notin \varphi(\partial\Omega)$, where $\partial\Omega$ denotes the boundary of Ω. The point q is said to be *regular* if either $\varphi^{-1}(q) = \emptyset$ or all points $\tilde{\mathcal{I}}^* \in \varphi^{-1}(q)$ return invertible $\nabla_{\tilde{\mathcal{I}}}\varphi(\tilde{\mathcal{I}}^*)$. Otherwise, q is called *critical*. The map $\mathcal{B} : C^1(\Omega) \times \Omega \times \mathbb{R}^5 \to \mathbb{Z}$ given by

$$\mathcal{B}(\varphi, \Omega, q) := \begin{cases} \sum_{\tilde{\mathcal{I}}^* \in \varphi^{-1}(q)} \operatorname{sign} \det \nabla_{\tilde{\mathcal{I}}}\varphi(\tilde{\mathcal{I}}^*), & q \text{ regular} \\ \mathcal{B}(\varphi, \Omega, \tilde{q}), & q \text{ critical},\ \tilde{q} \text{ regular},\ \|q - \tilde{q}\| < \inf_{s \in \varphi(\partial\Omega)} \|q - s\| \end{cases} \tag{3.10}$$

defines the *Brouwer degree* of φ in Ω with respect to a reference point q. When especially $\tilde{\mathcal{I}} = 0$ is isolated in the neighborhood Ω, the map

$$\operatorname{ind}(\varphi, 0) := \mathcal{B}(\varphi, \Omega, 0) \tag{3.11}$$

defines the *index* of φ at the isolated singular value $\tilde{\mathcal{I}} = 0$. According to [37,38], $(\mathcal{R}_{\mathrm{TT}} = 1, \tilde{\mathcal{I}} = 0)$ *is a branching point when* $\operatorname{ind}(\varphi, 0)$ *changes value around* $\mathcal{R}_{\mathrm{TT}} = 1$.

In case $\mathcal{R}_{\mathrm{TT}} < 1$, the fact that the matrix $\mathcal{F}\mathcal{V}^{-1}$ has eigenvalues 0 of algebraic multiplicity 2 also simple eigenvalues $\mathcal{R}_{\mathrm{TT}}$ and $\mathcal{R}_{\mathrm{TT}} \cdot (-1/2 \pm \sqrt{3}i/2)$ yields $\det \nabla_{\tilde{\mathcal{I}}}\varphi(0) = \det(\mathrm{id} - \mathcal{F}\mathcal{V}^{-1}) = \Pi_k(1 - \lambda_k) > 0$ for all the aforementioned eigenvalues λ_k. The preceding result stems from the fact the multiplication of complex conjugate numbers always returns a positive number. In case $\mathcal{R}_{\mathrm{TT}} > 1$, it is not difficult to show under the same way that $\det \nabla_{\tilde{\mathcal{I}}}\varphi(0) < 0$. Now we can specify Ω to span a sufficiently small range from $\tilde{\mathcal{I}} = 0$ and $\mathcal{R}_{\mathrm{TT}} \neq 1$ such that $\varphi(\tilde{\mathcal{I}}) = \varphi(0) + \nabla_{\tilde{\mathcal{I}}}\varphi(0) \cdot \tilde{\mathcal{I}} + \mathcal{O}(\|\tilde{\mathcal{I}}\|^2) \approx \tilde{\mathcal{I}} - \mathcal{F}\mathcal{V}^{-1}\tilde{\mathcal{I}}$, i.e., $\tilde{\mathcal{I}} = 0$ becomes isolated in Ω by the non-singularity of $\mathrm{id} - \mathcal{F}\mathcal{V}^{-1}$. The index of φ at the singular value $\tilde{\mathcal{I}} = 0$ is then given by

$$\operatorname{ind}(\varphi, 0) = \operatorname{sign} \det \nabla_{\tilde{\mathcal{I}}}\varphi(0) = \begin{cases} 1, & \mathcal{R}_{\mathrm{TT}} < 1 \\ -1, & \mathcal{R}_{\mathrm{TT}} > 1 \end{cases}.$$

This confirms that $(\mathcal{R}_{\mathrm{TT}} = 1, \tilde{\mathcal{I}} = 0)$ is indeed a branching point.

Our next step is to see if the local branch around $\mathscr{E}_{\mathrm{TTD}}$ is positive, indicating a continuum of coexistence equilibria. The idea follows from taking an asymptotic expansion of $\mathcal{R}_{\mathrm{TT}}$ from 1 [39,40], which will extend the local branch up to the boundary of Ω. After division by $\mathcal{R}_{\mathrm{TT}}$, the expansion takes the form

$$1 = \frac{1}{\mathcal{R}_{\mathrm{TT}}} + \frac{\mathcal{R}}{\mathcal{R}_{\mathrm{TT}}}\varepsilon + \mathcal{O}(\varepsilon^2), \quad 0 < \varepsilon \ll 1. \tag{3.12}$$

The coefficient of the first-order term $\mathcal{R}$ will determine if the branch takes off in the increment of $\mathcal{R}_{\mathrm{TT}}$ (in case positive, returning a forward bifurcation) or in the decrement of $\mathcal{R}_{\mathrm{TT}}$ (in case negative, a backward bifurcation). Owing to this expansion, the branch $\tilde{\mathcal{I}}$ takes the expression

$$\tilde{\mathcal{I}} = \psi_1\varepsilon + \psi_2\varepsilon^2 + \mathcal{O}(\varepsilon^3) \tag{3.13}$$

for yet unknown ψ_1 and ψ_2. Now we can substitute the preceding two expressions in the coefficient of $-\mathcal{F}\mathcal{V}^{-1}$ and Eq. (3.9) to have

$$\begin{aligned} 0 = &\left[\psi_1\varepsilon + \psi_2\varepsilon^2 + \mathcal{O}(\varepsilon^3)\right] - \left[\frac{1}{\mathcal{R}_{\mathrm{TT}}} + \frac{\mathcal{R}}{\mathcal{R}_{\mathrm{TT}}}\varepsilon + \mathcal{O}(\varepsilon^2)\right]\mathcal{F}\mathcal{V}^{-1}\left[\psi_1\varepsilon + \psi_2\varepsilon^2 + \mathcal{O}(\varepsilon^3)\right] \\ &- F_2\left(\psi_1\varepsilon + \psi_2\varepsilon^2 + \mathcal{O}(\varepsilon^3)\right) + \mathcal{O}(\varepsilon^3). \end{aligned}$$

On vanishing the first-order term (ε), we obtain

$$\mathcal{F}\mathcal{V}^{-1}\psi_1 = \mathcal{R}_{\mathrm{TT}}\psi_1. \tag{3.14}$$

This implies that ψ_1 is the right eigenvector of $\mathcal{F}\mathcal{V}^{-1}$ associated to $\mathcal{R}_{\mathrm{TT}}$, which is unique up to scalar multiplication. For further use, let us reveal the explicit formulations of the right as well as left eigenvector. They are given by

$$\psi_1 = \begin{pmatrix} \mathcal{R}_{\mathrm{TT}}^{-2} \cdot \frac{A_{max}}{k_c\delta_7} \cdot \frac{gM_1}{-\mathcal{J}_{77}} \\ \mathcal{R}_{\mathrm{TT}}^{-3} \cdot \frac{kV_1}{-\mathcal{J}_{55}} \cdot \frac{A_{max}}{k_c\delta_7} \cdot \frac{gM_1}{-\mathcal{J}_{77}} \\ \mathcal{R}_{\mathrm{TT}}^{-1} \cdot \frac{A_{max}}{k_c\delta_7} \\ \mathcal{R}_{\mathrm{TT}} \cdot \frac{-\mathcal{J}_{88}}{\alpha(T_1+I_1)} \\ 1 \end{pmatrix} \quad \text{and} \quad \xi_1 = \begin{pmatrix} 0 \\ 0 \\ \mathcal{R}_{\mathrm{TT}}^{-1} \cdot \frac{\delta_6}{-\mathcal{J}_{77}} \\ \mathcal{R}_{\mathrm{TT}} \cdot \frac{-\mathcal{J}_{88}}{\alpha(T_1+I_1)} \\ 1 \end{pmatrix}$$

respectively.

To reveal $\mathcal{R}$, we can multiply the second-order term (ε^2) with $\xi_1^\top$ from the left such that

$$\underbrace{\left[\xi_1^\top - \frac{1}{\mathcal{R}_{\mathrm{TT}}}\xi_1^\top\mathcal{F}\mathcal{V}^{-1}\right]}_{=0}\psi_2 - \mathcal{R}\xi_1^\top\psi_1 - \xi_1^\top F_2(\psi_1) = 0. \tag{3.15}$$

This results in

$$\mathcal{R} = -\frac{\xi_1^\top F_2(\psi_1)}{\xi_1^\top\psi_1}. \tag{3.16}$$

The preceding expression may look simple, however cannot be simplified in such a way that the sign is apparent due to the complexity of F_2. We reduce the degree of analyticity by fixing all the parameters except ϵ_{RT} and ϵ_P according to Tab. 1, which is then in line with the aim of this section. Since the asymptotic expansion is concerned with the local behavior of both $\mathcal{R}_{\mathrm{TT}}$ around 1 and the corresponding equilibria, it suffices to check the value of $\mathcal{R}$ for ϵ_{RT} and ϵ_P from which $\mathcal{R}_{\mathrm{TT}}$ varies around 1.

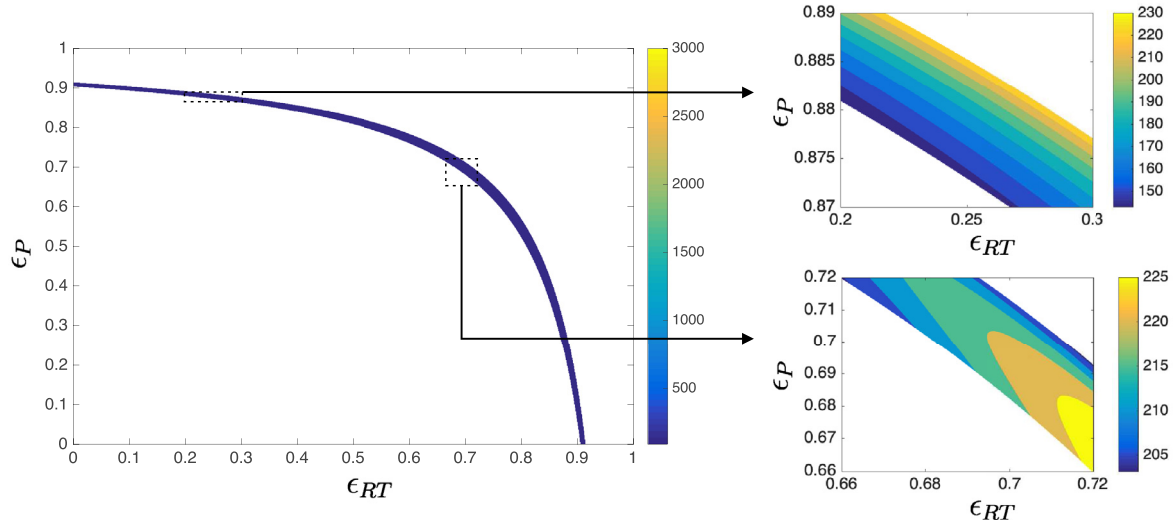

Fig. 3.1. Numerical values of $\mathcal{R}$ on the regime $0.93 \le \mathcal{R}_{\mathrm{TT}} \le 1.1$ and on two domain snippets of $(\epsilon_{RT}, \epsilon_P)$. The entire regime has been checked for the positivity of $\mathcal{R}$.

Fig. 3.1 graphically guarantees the positivity $\mathcal{R}$ in a neighborhood of $(\epsilon_{RT}, \epsilon_P)$ where $\mathcal{R}_{\mathrm{TT}} = 1$. The asymptotic expansions (3.12)–(3.13) under a positive $\mathcal{R}$ thus indicate that $\tilde{\mathcal{I}}$ increases with a positive initial direction ψ_1 and so does $\mathcal{R}_{\mathrm{TT}}$, as ε slightly increases from 0. Putting back the original variable $\mathcal{I} = \mathcal{V}^{-1}\tilde{\mathcal{I}}$, we obtain the existence of a unique positive local branch

$$\mathcal{I} = \mathcal{V}^{-1}\psi_1\varepsilon + \mathcal{O}(\varepsilon^2) \quad \text{where} \quad \partial_{\mathcal{R}_{\mathrm{TT}}}\mathcal{I}|_{\mathcal{R}_{\mathrm{TT}}=1} = \frac{\mathcal{V}^{-1}\psi_1}{\mathcal{R}} > 0. \tag{3.17}$$

This indicates the coexistence of T1D and HIV infection equilibrium in the direction of increasing $\mathcal{R}_{\mathrm{TT}}$ from 1. Due to complexity, this section scopes out only the existence of this equilibrium, leaving the local stability as a subject of numerical bifurcation analysis in Section 4. For interested readers, an idea for proving the local stability is to substitute an equilibrium with a certain ε from (3.17) to the Jacobian matrix. The state values of T, V, I, M can be found from those of M_a, M_i, and B_a, again, in terms of ε. In return, the Jacobian matrix also forms an asymptotic expansion of ε with the leading order $\mathcal{J}(\mathscr{E}_{\mathrm{T1D}})$ (matrix coefficient of ε^0), which apparently has negative first four eigenvalues for a sufficiently small ε. We can perturb $\mathcal{R}_{\mathrm{TT}}$ above one and use Roché's Theorem for the characteristic polynomial of the Jacobian matrix such that all eigenvalues stay in the open left-half plane in $\mathbb{C}$ except the one that corresponds to $\mathcal{R}_{\mathrm{TT}}$. Showing the negative real part of this last eigenvalue requires Taylor expansion of a simple eigenvalue of a perturbed matrix [41]. The final step is to find a negative upper bound of the expansion in the first-order of ε.

3.4. What drives to T1D & HIV infection coexistence the most

This section is devoted to determining which treatment between reverse transcriptase inhibitor and protease inhibitor is more effective in reducing the HIV viral load, before T1D–HIV coexistence. As far as the T1D-free equilibrium $\mathscr{E}_{\mathrm{T1D}}$ is concerned, we have seen that the state T_1 increases while V_1 and I_1 walk toward vanishing as ϵ_{RT} and ϵ_P increase simultaneously. Therefore, increasing ϵ_{RT} and ϵ_P is 'good' in terms of reducing the viral load but 'bad' in terms of discovering coexistence. Suppose that ϵ_{RT} is increased from its current value to a certain percentage ε. This is equivalent to $\epsilon_{RT} \mapsto \epsilon_{RT} + \varepsilon\epsilon_{RT}$. Accordingly, the ratio $(\epsilon_{RT} + \varepsilon\epsilon_{RT})/\epsilon_{RT} = 1 + \varepsilon$ gives the comparison between the values of ϵ_{RT} posterior and prior to the change, where ε serves as the gain percentage. Note that the increase by percentage is more technically sound for a general comparison as parameters may live in disparate scales. Applying the partial changes to both ϵ_{RT} and ϵ_P, the response variable $\mathcal{R}_{\mathrm{TT}} = \mathcal{R}_{\mathrm{TT}}(\epsilon_{RT}, \epsilon_P)$ in turn perturbs to new values. The explicit formula in (3.7) also hints that $\mathcal{R}_{\mathrm{TT}} = \mathcal{R}_{\mathrm{TT}}(u)$ where $u := (1 - \epsilon_{RT})(1 - \epsilon_P)$. Taking Taylor expansions of $\mathcal{R}_{\mathrm{TT}}$ yields

$$\frac{\mathcal{R}_{\mathrm{TT}}(\epsilon_{RT} + \varepsilon\epsilon_{RT}, \epsilon_P)}{\mathcal{R}_{\mathrm{TT}}(\epsilon_{RT}, \epsilon_P)} = 1 + \frac{\partial_{\epsilon_{RT}}\mathcal{R}_{\mathrm{TT}}(\epsilon_{RT}, \epsilon_P)}{\mathcal{R}_{\mathrm{TT}}(\epsilon_{RT}, \epsilon_P)}\epsilon_{RT}\varepsilon + \mathcal{O}(\varepsilon^2) = 1 - \frac{\mathcal{R}'_{\mathrm{TT}}(u)(1 - \epsilon_P)}{\mathcal{R}_{\mathrm{TT}}(\epsilon_{RT}, \epsilon_P)}\epsilon_{RT}\varepsilon + \mathcal{O}(\varepsilon^2),$$
$$\frac{\mathcal{R}_{\mathrm{TT}}(\epsilon_{RT}, \epsilon_P + \varepsilon\epsilon_P)}{\mathcal{R}_{\mathrm{TT}}(\epsilon_{RT}, \epsilon_P)} = 1 + \frac{\partial_{\epsilon_P}\mathcal{R}_{\mathrm{TT}}(\epsilon_{RT}, \epsilon_P)}{\mathcal{R}_{\mathrm{TT}}(\epsilon_{RT}, \epsilon_P)}\epsilon_P\varepsilon + \mathcal{O}(\varepsilon^2) = 1 - \frac{\mathcal{R}'_{\mathrm{TT}}(u)(1 - \epsilon_{RT})}{\mathcal{R}_{\mathrm{TT}}(\epsilon_{RT}, \epsilon_P)}\epsilon_P\varepsilon + \mathcal{O}(\varepsilon^2).$$

When the gain percentage ε is sufficiently small, the first-order terms of ε in the above expressions take the lead in determining the loss or gain in $\mathcal{R}_{\mathrm{TT}}$. In other words, $\mathcal{R}_{\mathrm{TT}}$ is more sensitive in the first-order of the gain percentage ε to the decrement of ϵ_{RT} than ϵ_P in the regime

$$\left|-\frac{\mathcal{R}'_{\mathrm{TT}}(u)(1 - \epsilon_P)}{\mathcal{R}_{\mathrm{TT}}(\epsilon_{RT}, \epsilon_P)}\epsilon_{RT}\right| > \left|-\frac{\mathcal{R}'_{\mathrm{TT}}(u)(1 - \epsilon_{RT})}{\mathcal{R}_{\mathrm{TT}}(\epsilon_{RT}, \epsilon_P)}\epsilon_P\right| \iff (1 - \epsilon_P)\epsilon_{RT} > (1 - \epsilon_{RT})\epsilon_P \iff \epsilon_{RT} > \epsilon_P. \tag{3.18}$$

The literature, e.g. [42,43], often calls the first-order terms of the gain percentage the *first-order elasticity indices*. Based on (3.18), our model highlights the importance of maintaining the efficacies of reverse transcriptase inhibitor and protease inhibitor at the same level, i.e., $\epsilon_{RT} = \epsilon_P$. For the sake of the reader, we present the numerical values of the first-order elasticity indices in Fig. 3.2. Having positive index values on the regime $\mathcal{R}_{\mathrm{TT}} < 1$ leads to conclude that $\mathcal{R}_{\mathrm{TT}}$ increases in the direction of increasing both ϵ_{RT} and ϵ_P. The elasticity index $\partial_{\epsilon_{RT}}\mathcal{R}_{\mathrm{TT}}\epsilon_{RT}/\mathcal{R}_{\mathrm{TT}} = 2.5$ means that under the increase of $\varepsilon = 10\%$ in ϵ_{RT}, the reproduction number $\mathcal{R}_{\mathrm{TT}}$ experiences an increase of approximately 25% from its current value.

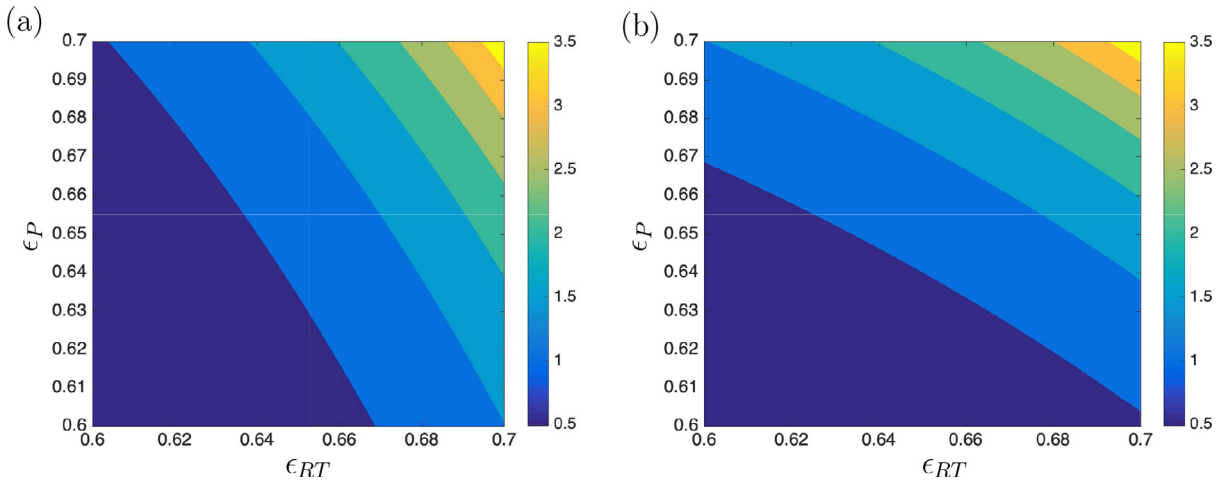

Fig. 3.2. Numerical values of the first-order elasticity indices $\partial_{\epsilon_{RT}} \mathcal{R}_{\mathrm{TT}} \epsilon_{RT} / \mathcal{R}_{\mathrm{TT}}$ (panel a) and $\partial_{\epsilon_P} \mathcal{R}_{\mathrm{TT}} \epsilon_P / \mathcal{R}_{\mathrm{TT}}$ (panel b) on the domain snippet $(\epsilon_{RT}, \epsilon_P) \in [0.6, 0.7]^2$ where $\mathcal{R}_{\mathrm{TT}} < 1$. The other parameter values are given in Table 1.

Table 2.1
Parameters used in the numerical simulations model (2.2)–(2.10).

Parameter	Value	Units	Reference
s	1.0×10^4	$\mathrm{ml}^{-1}\ \mathrm{day}^{-1}$	[30]
p	0.03	day^{-1}	[31]
$T_{\max}$	1.5×10^6	ml^{-1}	[31]
δ_1	0.01	day^{-1}	[30]
δ_2	0.8	day^{-1}	[32]
δ_3	0.8	day^{-1}	[25]
δ_4	0.1	day^{-1}	[25]
δ_5	0.1	day^{-1}	[33]
δ_6	0.5	day^{-1}	[25]
δ_7	25.0	day^{-1}	[25]
c	23.0	day^{-1}	[30]
k	3.92×10^{-9}	$\mathrm{ml\ day}^{-1}$	[30]
N_1	2.8×10^3	————	[34]
N_2	1.0×10^3	————	[33]
J	5.0×10^4	$\mathrm{ml}^{-1}\ \mathrm{day}^{-1}$	[25]
b	0.09	day^{-1}	[25]
g	1.0×10^{-5}	$\mathrm{ml}^{-1}\ \mathrm{day}^{-1}$	[25]
f_1	2.0×10^{-6}	$\mathrm{ml}^{-1}\ \mathrm{day}^{-1}$	[25]
f_2	1.0×10^{-6}	$\mathrm{ml}^{-1}\ \mathrm{day}^{-1}$	[25]
f_3	1.5×10^{-4}	$\mathrm{ml}^{-1}\ \mathrm{day}^{-1}$	[25]
e_1	1.0×10^{-8}	day^{-1}	[25]
e_2	8.0×10^{-8}	day^{-1}	[25]
e_3	8.0×10^{-8}	day^{-1}	[25]
$A_{\max}$	2.0×10^5	$\mathrm{ml}^{-1}\ \mathrm{day}^{-1}$	[25]
k_c	1.5×10^{-2}	————	[25]
α	2.56×10^{-11}	day^{-1}	[25]
ϵ_{RT}	[0,1]	————	Varied
ϵ_P	[0,1]	————	Varied

4. Numerical investigation of the HIV-diabetes model via path-following methods

In this section, our main concern will be to investigate the behavior of both disease-free (i.e. with no HIV) and endemic equilibria when the main disease control parameters are varied. These are ϵ_{RT} and ϵ_P, which represent the efficacy of reverse transcriptase inhibitors (RTI) and protease inhibitors (PI) treatment, respectively, whose purpose is to reduce the HIV viral load below the limit of detection (50 HIV-1 RNA copies/ml blood, for the US-RT-PCR assay). Moreover, before carrying out this analysis, it is convenient to introduce a re-scaling of the model (2.2) as specified below:

$$
\begin{aligned}
&\widetilde{T} := \frac{T}{T_{max}}, && \widetilde{I} := \frac{I}{T_{max}}, && \widetilde{V} := \frac{V}{T_{max}}, && \widetilde{M} := \frac{M}{T_{max}}, && \widetilde{M}_a := \frac{M_a}{T_{max}},\\
&\widetilde{M}_i := \frac{M_i}{T_{max}}, && \widetilde{B}_a := \frac{B_a}{T_{max}}, && \widetilde{B}_n := \frac{B_n}{T_{max}}, && \widetilde{C} := \frac{C}{T_{max}}, && \widetilde{s} := \frac{s}{T_{max}},\\
&\widetilde{k} := k \cdot T_{max}, && \widetilde{J} := \frac{J}{T_{max}}, && \widetilde{g} := g \cdot T_{max}, && \widetilde{e}_1 := e_1 \cdot T_{max}, && \widetilde{e}_2 := e_2 \cdot T_{max},\\
&\widetilde{e}_3 := e_3 \cdot T_{max}, && \widetilde{A}_{max} := \frac{A_{max}}{T_{max}}, && \widetilde{k}_c := \frac{k_c}{T_{max}}, && \widetilde{f}_1 := f_1 \cdot T_{max}, && \widetilde{f}_2 := f_2 \cdot T_{max},\\
&\widetilde{f}_3 := f_3 \cdot T_{max}, && \widetilde{\alpha} := \alpha \cdot T_{max}.
\end{aligned}
$$

The numerical investigation will be carried out using the scaled variables and parameters shown above, but the results will be presented in the original scales for the sake of clarity. On the other hand, for the purpose of investigating the effect of the HIV treatment

on the system (controlled by the parameters ϵ_P and ϵ_{RT}), we will introduce certain solution measures that will help quantify the presence of HIV and type 1 diabetes in the model. Suppose $\left(T^0, I^0, V^0, M^0, M_a^0, M_i^0, B_a^0, B_n^0, C^0\right)$ is an (biologically meaningful) equilibrium of system (2.2)-(2.10). Then we define

$$M_{\text{HIV}} = \sqrt{\left(I^0\right)^2 + \left(V^0\right)^2 + \left(M_i^0\right)^2}, \quad M_{\text{T1D}} = \sqrt{\left(B_a^0\right)^2 + \left(B_n^0\right)^2 + \left(C^0\right)^2}, \tag{4.1}$$

which will be used to identify different (co)infection scenarios, depending on whether the above introduced quantities are different from zero or not.

After these preliminary remarks, we can now carry out the numerical study of the disease-free and endemic equilibria of the HIV-diabetes model (2.2)-(2.10). Specifically, we will investigate how the main control parameters affect the stability of the equilibria of the model via the continuation platform COCO [44]. The starting point of the numerical investigation is assumed to be a diabetes-free state where HIV is present in the body. This scenario is simulated in Fig. 4.1, which depicts the dynamical response of the T1D-HIV model (2.2)-(2.10), computed for the parameter values given in Table 1 (solid line), with $\epsilon_P = \epsilon_{RT} = 0$ (i.e. no HIV treatment). For the given parameter set, the assumed (nonzero) initial conditions lead the system to a disease-free steady state, that is, with no HIV and no type 1 diabetes (T1D). If now the underlying patient suffers an increase in the aggressiveness of the diseases, simulated by a growth in the cytokines production rate α (from 2.56×10^{-11} to 2.71×10^{-11}) and the HIV infection rate k (from 3.92×10^{-9} to 6.67×10^{-8}), the system settles down to a steady state with HIV in the body and no T1D. This solution is represented by the dashed line in Fig. 4.1, and will be used as the starting point for our numerical investigation.

Let us begin our study with the T1D-free equilibrium with HIV described above, obtained for $k = 6.67 \times 10^{-8}$ and $\alpha = 2.71 \times 10^{-11}$. We will investigate first how this equilibrium is affected by the HIV treatment based on reverse transcriptase inhibitors, controlled by the parameter $\epsilon_{RT} \in [0, 1]$. The numerical continuation of the steady state with respect to this parameter is shown in Fig. 4.2. As can be seen from panel (a), a low value of ϵ_{RT} allows a high presence of HIV, measured by the quantity M_{HIV} defined in (4.1). Moreover, panel (c) displays the behavior of M_{T1D} (also defined in (4.1)), which quantifies the presence of T1D in the system. These two pictures thus indicate that for low levels of HIV treatment the original situation persists. If ϵ_{RT} is increased, a critical value $\epsilon_{RT} \approx 0.9093$ (labeled BP1 in the figure) is detected, where the T1D-free equilibrium loses stability and a another state emerges, with both HIV and type 1 diabetes in the system, meaning that the underlying patient has developed the latter disease as a result of the HIV treatment. This critical behavior

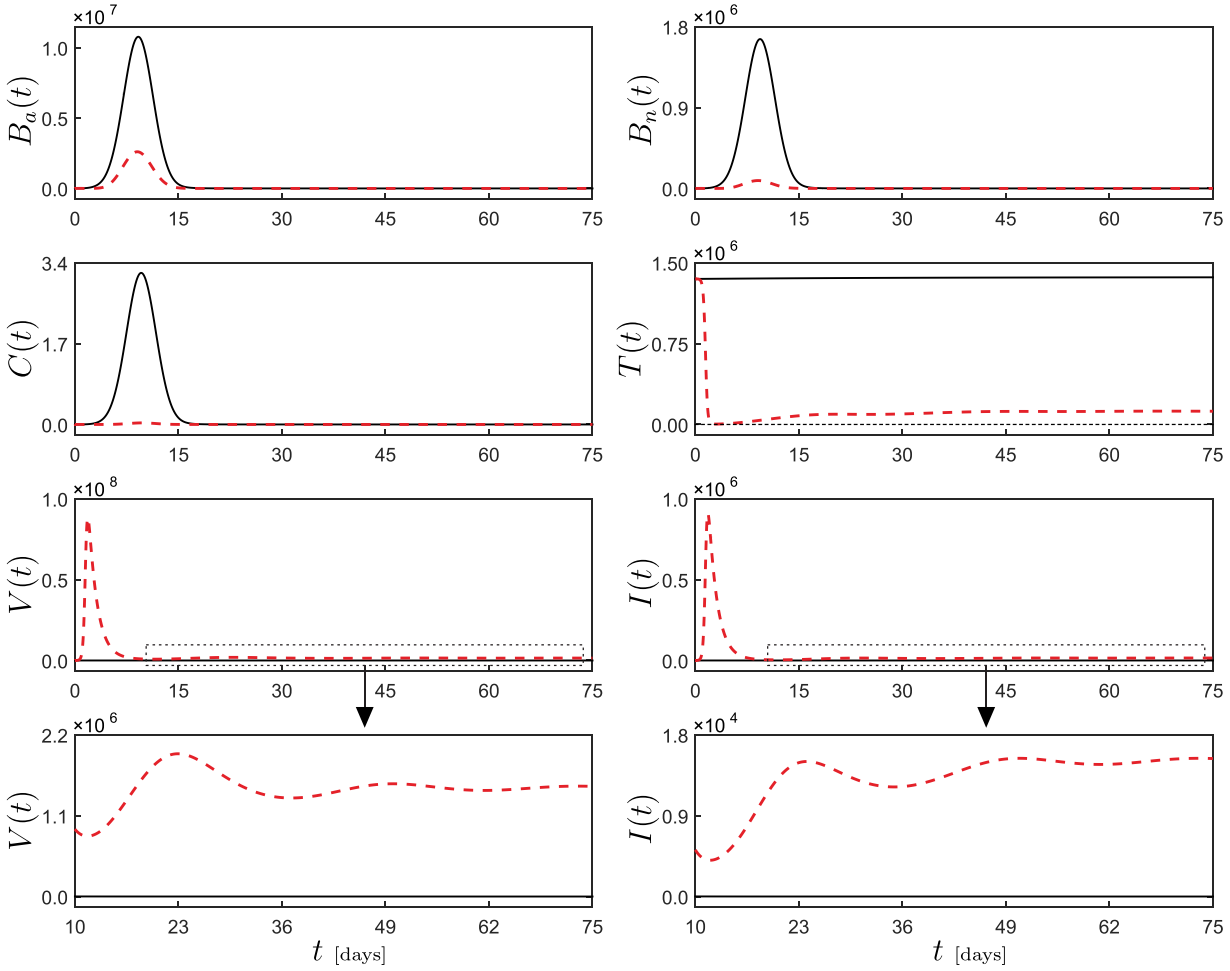

Fig. 4.1. Dynamical response of the T1D-HIV model (2.2)-(2.10), computed for the parameter values given in Table 1 (solid line), with $\epsilon_P = \epsilon_{RT} = 0$ (no HIV treatment). The dashed line corresponds to the case $k = 6.67 \times 10^{-8}$ and $\alpha = 2.71 \times 10^{-11}$. The picture shows time series for healthy CD4$^+$ T cells ($T(t)$), HIV-infected CD4$^+$ T cells ($I(t)$), HIV viral concentration ($V(t)$), apoptotic β-cells ($B_a(t)$), necrotic β-cells ($B_n(t)$) and cytokines ($C(t)$). Both numerical simulations are computed with the initial conditions $T(0) = 1.35 \times 10^6$, $I(0) = 1.50 \times 10^2$, $V(0) = 7.50 \times 10^3$, $M(0) = 4.50 \times 10^4$, $M_a(0) = 3.00 \times 10^4$, $M_i(0) = 45$, $B_a(0) = 1.20 \times 10^3$, $B_n(0) = 1.50 \times 10^2$, $C(0) = 9.60 \times 10^{-4}$.

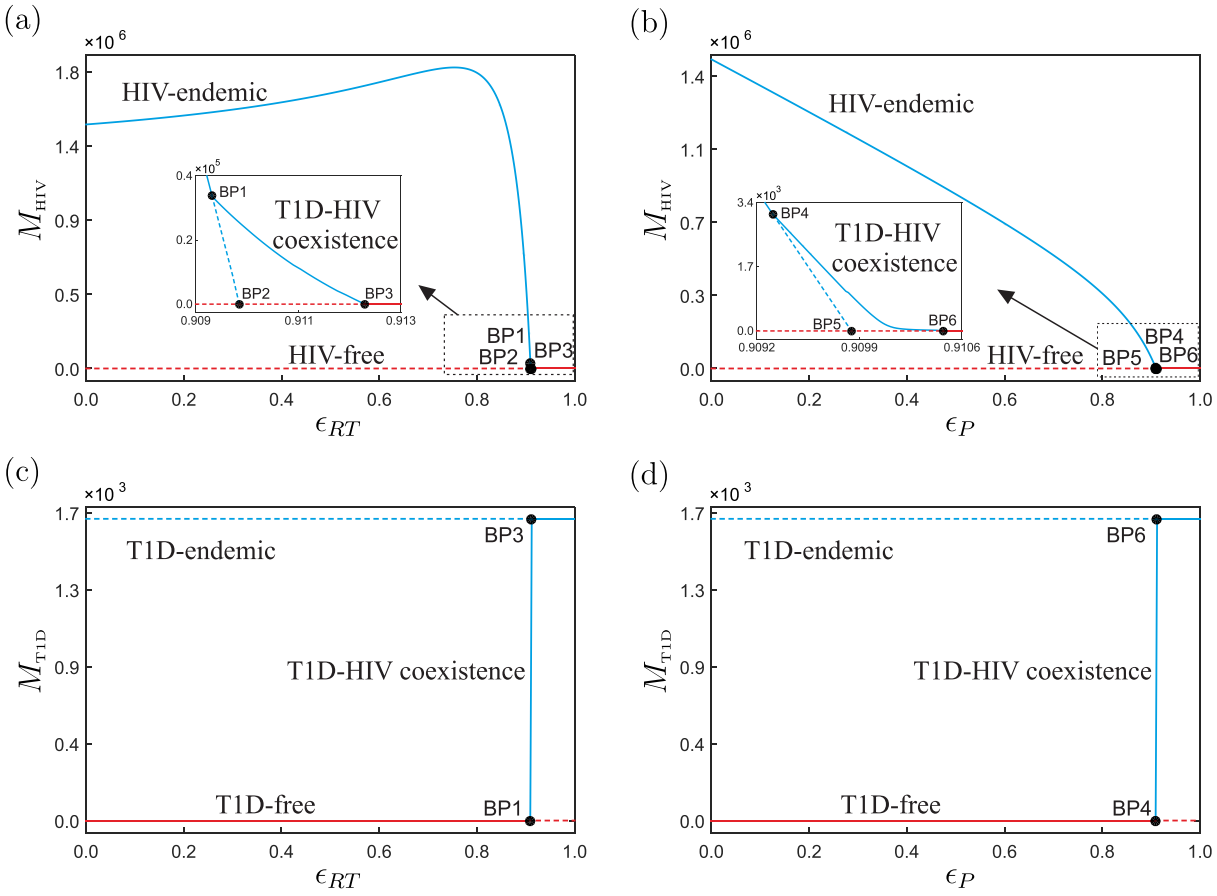

Fig. 4.2. Numerical continuation of equilibria of the T1D-HIV model (2.2)-(2.10) with respect to ϵ_{RT} and ϵ_P using the parameter values employed in Fig. 4.1, with $k = 6.67 \times 10^{-8}$ and $\alpha = 2.71 \times 10^{-11}$. Stable and unstable equilibria are depicted with solid and dashed lines, respectively. The vertical axes present the solution measures defined in (4.1). During the computations, a series of branching points are detected for $\epsilon_{RT} \approx 0.9093$ (BP1), $\epsilon_{RT} \approx 0.9098$ (BP2), $\epsilon_{RT} \approx 0.9123$ (BP3) (depicted in panels (a) and (c)) and $\epsilon_P \approx 0.9093$ (BP4), $\epsilon_P \approx 0.9098$ (BP5), $\epsilon_P \approx 0.9105$ (BP6) (depicted in panels (b) and (d)).

corresponds to a branching point (of transcritical type) [45,46], also known in the Mathematical Biology field as a forward bifurcation [47,48]. On the other hand, Fig. 4.2(a) reveals a decreasing tendency of HIV presence in the system as ϵ_{RT} grows, with a critical value $\epsilon_{RT} \approx 0.9123$ (BP3), where the HIV viral load becomes zero. In this way, the bifurcation points BP1 and BP3 define a coexistence window for HIV and T1D, $\epsilon_{RT} \in (0.9093, 0.9123)$, in which the patient suffers from two diseases (HIV and T1D), with T1D developed as a product of the HIV treatment. As can be seen in panels (a) and (c), for higher values of ϵ_{RT} the system dynamics is now characterized by a steady state with type 1 diabetes and no HIV in the body. An analogous scenario is encountered if now ϵ_{RT} is set to zero and ϵ_P is allowed to vary freely, i.e., HIV is treated using protease inhibitors, see Fig. 4.2(b) and (d).

As observed in Fig. 4.2, the HIV viral load can be effectively controlled by the parameters ϵ_P and ϵ_{RT}. For both type of treatments, however, our numerical investigation established a critical window where coexistence takes place, due to which a patient may be in danger owing to the presence of both diseases (HIV and T1D). This critical window is characterized by two branching points, for instance the ones labeled BP1 and BP3 shown in Fig. 4.2(a). In this way, the system equilibria can be classified into three regimes as the control parameters ϵ_P, ϵ_{RT} vary: T1D-free with HIV, HIV-T1D coexistence and HIV-free with T1D.

In order to gain further insight into the system regimes discussed above, we will carry out a two-parameter continuation with respect to ϵ_P and ϵ_{RT} of the branching points BP1 and BP3 shown in Fig. 4.2(a), which define the boundary points of the above mentioned regimes. In this way, we can compute two curves (shown in Fig. 4.3(a)) labeled ℓ_1 and ℓ_2 corresponding to the numerical continuation of the branching points BP1 and BP3, respectively. These curves divide the parameter space $\epsilon_{RT} - \epsilon_P$ locally into three regions: T1D-free with HIV (plotted in yellow), HIV-T1D coexistence (plotted in red) and HIV-free with T1D (plotted in blue), as described earlier. This means, for instance, that if we choose a specific treatment represented by some combination of $(\epsilon_{RT}, \epsilon_P)$, we can determine before hand which of the possible disease scenarios will be expected in the long run. Therefore, depending on a particular profile of a patient a treatment can be decided. For instance, an HIV-patient with high risk of developing type 1 diabetes should receive a treatment taken from the yellow region shown in Fig. 4.3(a), with the operation point reasonably away from the red area corresponding to the coexistence scenario. To illustrate this, three sample cases are simulated in Fig. 4.3(b), corresponding to the test points P1 ($\epsilon_{RT} = 0.897$, $\epsilon_P = 0.1$, yellow region), P2 ($\epsilon_{RT} = 0.899$, $\epsilon_P = 0.115$, red region) and P3 ($\epsilon_{RT} = 0.901$, $\epsilon_P = 0.13$, blue region). As can be seen from the time plots in Fig. 4.3(b), the predicted behavior is confirmed. At P1 (red time series) the HIV treatment is not sufficiently strong in order to reduce the viral load, due to which the system settles down to a steady state with HIV persistence, while the state variables related to T1D decay to zero. The treatment provided by the test point P2 lies in the red region, whose numerical simulation is plotted in black. In this case we can observe a significant reduction in the HIV presence in the body, however, at the price of having developed type 1 diabetes. For the third point (lying in the blue region) HIV is effectively eradicated, as expected, but the T1D levels become even higher than in the previous two cases, see the time plot in blue depicted in Fig. 4.3(b).

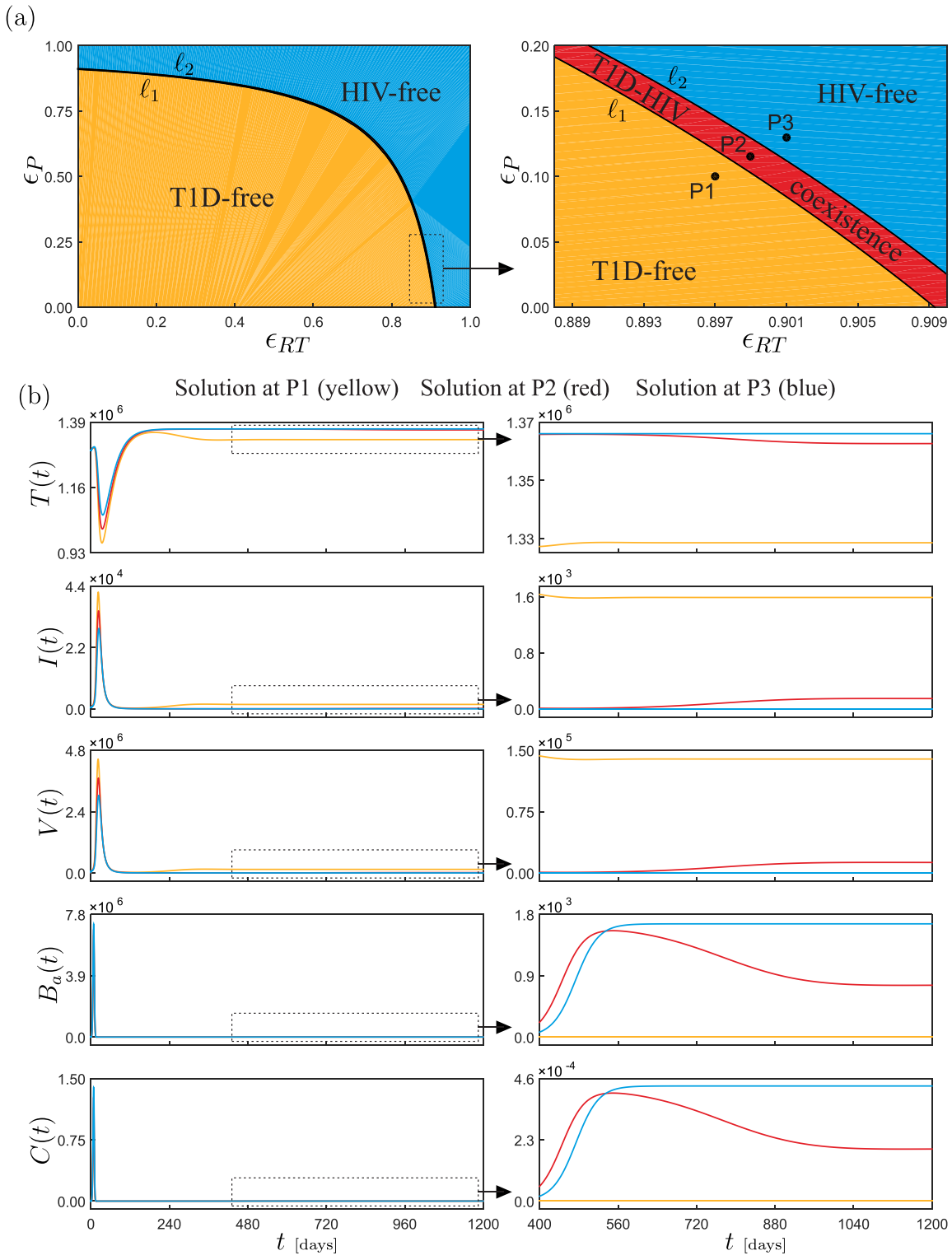

Fig. 4.3. (a) Two-parameter continuation of the branching point BP1 (curve labeled ℓ_1) and BP3 (curve labeled ℓ_2) found in Fig. 4.2(a), with respect to ϵ_{RT} and ϵ_P. The resulting curves divide the parameter space into three regions: one with HIV and no diabetes (yellow), one corresponding to HIV-diabetes coexistence (red) and one with diabetes and no HIV (blue). (b) System responses obtained at the test points P1 ($\epsilon_{RT} = 0.897$, $\epsilon_P = 0.1$, red curve), P2 ($\epsilon_{RT} = 0.899$, $\epsilon_P = 0.115$, black curve) and P3 ($\epsilon_{RT} = 0.901$, $\epsilon_P = 0.13$, blue curve). The right column of panel (b) shows enlargements of the boxed windows displayed on the left column. All numerical simulations are computed with the initial conditions $T(0) = 1.29 \times 10^6$, $I(0) = 5.40 \times 10^2$, $V(0) = 1.65 \times 10^4$, $M(0) = 5.25 \times 10^4$, $M_a(0) = 4.80 \times 10^4$, $M_i(0) = 4.50 \times 10^3$, $B_a(0) = 2.40 \times 10^3$, $B_n(0) = 4.35 \times 10^2$, $C(0) = 6.60 \times 10^{-3}$. (For interpretation of the references to colour in this figure legend, the reader is referred to the web version of this article.)

5. Concluding remarks

In this work we proposed a within-host model for the dynamics of T1D in HIV-infected patients, after immune restoration, and under HAART. The analysis of the model consisted in the study of the qualitative properties of the model. This was followed by the numerical simulations, in which was evaluated the response of the system as main control parameters, namely the effectiveness of the antiviral drugs reverse transcriptase inhibitors (ϵ_{RT}) and protease inhibitors (ϵ_P), were varied. The main goal was to reduce the HIV viral load below the limit of detection (50 HIV-1 RNA copies/mL blood). The one-parameter bifurcation analysis revealed the presence of branching points (BP1 and BP3) of transcritical (or forward) type, as ϵ_{RT} and ϵ_P varied. Furthermore, the bifurcating points BP1 and BP3 define a coexistence window, suggesting T1D developed as a product of the HIV treatment, which led to immune restoration.

During the numerical continuation in COCO, we have also monitored the behavior of T1D variables of interest, namely the cytokine concentration (C), the concentration of apoptotic β-cells (B_a) and the concentration of necrotic β-cells (B_n). Results show that the RTI and PI drugs influence the dynamics of T1D related cells (apoptotic and necrotic β-cells) and HIV. This suggests an association between HIV and T1D variables, which may provide useful insights for clinical practice, namely to devise adequate treatment protocols, according to patients' profiles. As a last comment, we should mention that this is a very simple model, which by itself suggests an association between ART treatment and the development of T1D. Nevertheless, the analysis is preliminary and clinical trials should be devised to provide real data to be fitted by the proposed model.

Credit author Statement

All authors have contributed equally to the manuscript.

Declaration of Competing Interest

Not applicable.

Acknowledgments

The author CP was partially supported by CMUP, which is financed by national funds through FCT - Fundação para a Ciência e a Tecnologia, I.P., under the project with reference UIDB/00144/2020.

References

[1] Diabetes Teaching Center at the University of California, USA. Autoimmunity. Available at https://dtc.ucsf.edu/types-of-diabetes/type1/understanding-type-1-diabetes/autoimmunity;
[2] International Diabetes Federation. What is diabetes?Available at https://www.idf.org/aboutdiabetes/what-is-diabetes.html;
[3] World Health Organization. Diabetes fact sheet. Available at https://www.who.int/news-room/fact-sheets/detail/diabetes;
[4] Beyond Type 1. Typ1 1 Diabetes Statistics. Available at https://beyondtype1.org/type-1-diabetes-statistics/;
[5] Mobasseri M, Shirmohammadi M, Amiri T, Vahed N, Fard HH, Ghojazadeh M. Prevalence and incidence of type 1 diabetes in the world: a systematic review and meta-analysis. Health Promot Perspect 2020;10(2):98.
[6] International Diabetes Federation. Diabetes facts & figures. Available at https://www.idf.org/aboutdiabetes/what-is-diabetes/facts-figures.html;
[7] U.S. Department of Health & Human Services. What Are HIV and AIDS?Available at https://www.hiv.gov/hiv-basics/overview/about-hiv-and-aids/what-are-hiv-and-aids;
[8] World Health Organization. Hiv fact sheet. Available at https://www.who.int/news-room/fact-sheets/detail/hiv-aids;
[9] United Nations Programme on HIV/AIDS. HIV prevention. Available at https://www.unaids.org/en/topic/prevention;
[10] Abebe SM, Getachew A, Fasika S, Bayisa M, Demisse AG, Mesfin N. Diabetes mellitus among hiv-infected individuals in follow-up care at university of gondar hospital, northwest ethiopia. BMJ Open 2016;6(8).
[11] Ledergerber B, Furrer H, Rickenbach M, Lehmann R, Elzi L, Hirschel B, Cavassini M, Bernasconi E, Schmid P, Egger M, et al. Factors associated with the incidence of type 2 diabetes mellitus in hiv-infected participants in the swiss hiv cohort study. Clinical Infectious Diseases 2007;45(1):111–19.
[12] Galli L, Salpietro S, Pellicciotta G, Galliani A, Piatti P, Hasson H, et al. Risk of type 2 diabetes among hiv-infected and healthy subjects in italy. Eur J Epidemiol 2012;27(8):657–65.
[13] Guillen MA, Mejia FA, Villena J, Turin CG, Carcamo CP, Ticse R. Insulin resistance by homeostasis model assessment in hiv-infected patients on highly active antiretroviral therapy: cross-sectional study. Diabetology & metabolic syndrome 2015;7(1):1–6.
[14] Mahaffy JM, Edelstein-Keshet L. Modeling cyclic waves of circulating t cells in autoimmune diabetes. SIAM J Appl Math 2007;67(4):915–37.
[15] Magombedze G, Nduru P, Bhunu CP, Mushayabasa S. Mathematical modelling of immune regulation of type 1 diabetes. BioSystems 2010;102(2–3):88–98.
[16] Marinković T, Sysi-Aho M, Orešič M. Integrated model of metabolism and autoimmune response in β-cell death and progression to type 1 diabetes. PLoS ONE 2012;7(12):e51909.
[17] Nielsen KH, Pociot FM, Ottesen JT. Bifurcation analysis of an existing mathematical model reveals novel treatment strategies and suggests potential cure for type 1 diabetes. Mathematical medicine and biology: a journal of the IMA 2014;31(3):205–25.
[18] Carvalho AR, Pinto CM, de Carvalho JM. Fractional model for type 1 diabetes. In: Mathematical Modelling and Optimization of Engineering Problems. Springer; 2020. p. 175–85.
[19] Abdel-Khalek I, Moallem H, Fikrig S, Castells S. New onset diabetes mellitus in an hiv-positive adolescent. AIDS Patient Care STDS 1998;12(3):167–9.
[20] Takarabe D, Rokukawa Y, Takahashi Y, Goto A, Takaichi M, Okamoto M, Tsujimoto T, Noto H, Kishimoto M, Kaburagi Y, et al. Autoimmune diabetes in hiv-infected patients on highly active antiretroviral therapy. The Journal of Clinical Endocrinology & Metabolism 2010;95(8):4056–60.
[21] Shinji K, Hideaki K, Mitsuru H, Yuki H, Akihito T, Masashi S, et al. Case of newly onset type 1 diabetes after highly active antiretroviral therapy against HIV infection. J Diabetes Investig 2015;6(3):367–8.
[22] Shimoyama Y, Umegaki O, Ooi Y, Shigemoto S, Agui T, Kadono N, et al. Sudden, sharp turn in an aids patient's course following the onset of fulminant type 1 diabetes. Acta Med Okayama 2019;73(3):263–7.
[23] Lane KL, Moin T. Autoimmune diabetes in a patient with human immunodeficiency virus on anti-retroviral therapy with literature review. AACE Clinical Case Reports 2020;6(5):e201–6.
[24] Perelson AS, Neumann AU, Markowitz M, Leonard JM, Ho DD. HIV-1 Dynamics in vivo: virion clearance rate, infected cell life-span, and viral generation time. Science 1996;271(5255):1582–6.
[25] Marée AF, Kublik R, Finegood DT, Edelstein-Keshet L. Modelling the onset of type 1 diabetes: can impaired macrophage phagocytosis make the difference between health and disease? Philosophical Transactions of the Royal Society A: Mathematical, Physical and Engineering Sciences 2006;364(1842):1267–82.
[26] Hadjiandreou MM, Conejeros R, Wilson DI. Long-term hiv dynamics subject to continuous therapy and structured treatment interruptions. Chem Eng Sci 2009;64(7):1600–17.
[27] De Blasio BF, Bak P, Pociot F, Karlsen AE, Nerup J. Onset of type 1 diabetes: a dynamical instability. Diabetes 1999;48(9):1677–85.
[28] Kassem SA, Ariel I, Thornton PS, Scheimberg I, Glaser B. Beta-cell proliferation and apoptosis in the developing normal human pancreas and in hyperinsulinism of infancy. Diabetes 2000;49(8):1325–33.
[29] Bonner-Weir S, Aguayo-Mazzucato C, Weir GC. Dynamic development of the pancreas from birth to adulthood. Ups J Med Sci 2016;121(2):155–8.
[30] Conway JM, Perelson AS. Post-treatment control of hiv infection. Proceedings of the National Academy of Sciences 2015;112(17):5467–72.
[31] Lou J, Ruggeri T, Ma Z. Cycles and chaotic behavior in an aids-related cancer dynamic model in vivo. Journal of Biological Systems 2007;15(02):149–68.
[32] Dixit NM, Markowitz M, Ho DD, Perelson AS. Estimates of intracellular delay and average drug efficacy from viral load data of hiv-infected individuals under antiretroviral therapy. Antivir Ther 2004;9(2):237–46.
[33] Barker CT, Vaidya NK. Modeling hiv-1 infection in the brain. PLoS Comput Biol 2020;16(11):e1008305.
[34] Culshaw RV, Ruan S. A delay-differential equation model of hiv infection of cd4+ t-cells. Math Biosci 2000;165(1):27–39.
[35] van den Driessche P, Watmough J. Reproduction numbers and sub-threshold endemic equilibria for compartmental models of disease transmission. Math Biosci 2002;180:29–48.
[36] Crandall MG, Rabinowitz PH. Mathematical theory of bifurcation. In: Bifurcation Phenomena in Mathematical Physics and Related Topics. Springer; 1980. p. 3–46.
[37] Tian Ma and Shouhong Wang. Bifurcation theory and applications. World Scientific Press, Singapore; 2005.
[38] Alexander Krasnosel'skii and P. P. Zabreiko. Geometrical methods of nonlinear analysis. Springer-Verlag, Berlin; 1984.
[39] Wijaya KP, Páez Chávez J, Pochampalli R, Rockenfeller R, Aldila D, Götz T, et al. Food sharing and time budgeting in predator-prey interaction. Commun Nonlinear Sci Numer Simul 2021;97:105757.
[40] Al-Salman AM, Páez Chávez J, Wijaya KP. A modeling study of predator–prey interaction propounding honest signals and cues. Appl Math Model 2021;89(2):1405–17.
[41] Karow M, Kressner D. On a perturbation bound for invariant subspaces of matrices. SIAM J Matrix Anal Appl 2014;35(2):599–618.

[42] Saltelli A, Ratto M, Andres T, Campolongo F, Cariboni J, Gatelli D, et al. Global sensitivity analysis: the primer. John Wiley & Sons, US; 2008.
[43] Tomovic R, Vukobratovic M. General sensitivity theory. North-Holland, Netherlands; 1972.
[44] Dankowicz H, Schilder F. Recipes for continuation. Computational Science and Engineering. Philadelphia: SIAM; 2013.
[45] Guckenheimer J, Holmes P. Nonlinear oscillations, dynamical systems, and bifurcations of vector fields. Applied Mathematical Sciences, vol. 42. New York: Springer-Verlag; 1993. Fourth printing
[46] Govaerts W. Numerical methods for bifurcations of dynamical equilibria. Philadelphia: SIAM; 2000.
[47] Kribs-Zaleta CM, Velasco-Hernández JX. A simple vaccination model with multiple endemic states. Math Biosci 2000;164(2):183–201.
[48] van den Driessche P, Watmough J. A simple SIS epidemic model with a backward bifurcation. J Math Biol 2000;40(6):525–40.